International Journal of Technology

http://ijtech.eng.ui.ac.id

Research Article

Modification of Poly(ethylene Terephthalate) Track-Etched Membranes with Titanium Dioxide by Arc Physical Vapor Deposition

Ilya E. Kuklin[1], Ilya V. Korolkov[2,3*], Nikolai R. Barashev[1], Nikolai A. Khlebnikov[1], Aigerim Kh. Shakayeva[2,3], Nurdaulet Zhumanazar[2,3], Arman B. Yeszhanov[2,3], Evgeny V. Polyakov[4]

[1]Ural Federal University, 620002, Mira str. 19, Ekaterinburg, Russia

[2]The Institute of Nuclear Physics, 050032, Ibragimov str., 1, Almaty, Kazakhstan

[3]L.N. Gumilyov Eurasian National University, Satpaev str., 2, 010008 Astana, Kazakhstan

[4]Institute of Solid State Chemistry, UB RAS, 91, Pervomaiskaya str., 620108, Ekaterinburg, Russian Federation

[*]Corresponding author: i.korolkov@inp.kz; Tel.: +7-7172-342058; Fax: +7-7172-342078

Abstract: In this study, TiO_2 coatings were deposited on polyethylene terephthalate (PET) track-etched membranes using vacuum-arc ion-plasma deposition (Arc-PVD) at deposition times from 0.5 to 8 min to obtain multifunctional filtration materials. The influence of deposition parameters on membrane surface morphology, pore structure, roughness, crystallinity, mechanical properties, wettability, and photocatalytic activity was systematically investigated. Surface characterization by SEM and AFM revealed progressive pore constriction from 200 to 93 nm with increasing deposition time, accompanied by particle growth and changes in surface topography, reflected in increased roughness (1.7–4.1 nm) and waviness (4–25.2 nm). X-ray diffraction confirmed the formation of nanocrystalline anatase at shorter deposition times, while prolonged deposition (8 min) resulted in the appearance of a secondary brookite phase. Increasing the deposition time reduced the lattice strain and dislocation density, thereby improving the coating hardness and mechanical stability. Under UV irradiation, the TiO_2 coatings exhibited photocatalytic activity toward hydroquinone oxidation, achieving approximately 70–73% degradation after 14 h. The apparent reaction rate constant reached 5×10^{-5} s^{-1}, with maximum activity observed for the coating deposited for 120 s, which is comparable to the benchmark TiO_2 photocatalyst Degussa P25. Compared with conventional magnetron sputtering approaches, Arc-PVD provides a highly ionized plasma flux that enables deposition of dense nanostructured TiO_2 coatings with enhanced adhesion on temperature-sensitive polymer substrates while preserving pore connectivity. The ability to control pore geometry and impart photocatalytic functionality demonstrates the potential of Arc-PVD-modified track-etched membranes for antifouling, self-cleaning, and advanced water purification applications.

Keywords: Ion-plasma spraying; Photocatalytic activity; Surface modification; Track-etched membranes; Titanium dioxide; Vacuum-arc

1. Introduction

Recently, the functionalization of polymer membranes with nanostructured coatings has attracted significant attention due to the growing demand for high-performance separation materials with enhanced chemical, mechanical, and functional properties (Le et al., 2024; Leong et al., 2014). Among various coating materials, titanium dioxide (TiO_2) stands out for its unique combination of photocatalytic activity, chemical stability, and antibacterial effects (Leong et al., 2014; Li et al., 2023; Matsudo et al., 2024). These properties make TiO_2-modified membranes highly attractive for water purification and advanced filtration technologies.

https://doi.org/10.14716/ijtech.v17i4.8346
Received January 2026; Revised January 2026; Accepted June 2026

Polymer track-etched membranes (TeMs), fabricated by ion irradiation and subsequent chemical etching, represent a distinct class of separation materials characterized by a narrow pore size distribution, well-defined cylindrical pores, and tunable porosity (Apel, 2019; Apel et al., 2018; Vilenskii et al., 2013; Wen et al., 2016; Werber et al., 2016). Their unique structure offers excellent control over transport properties and selectivity, making TeMs valuable in microfiltration, membrane distillation (Kravets et al., 2025; Shakayeva et al., 2024b, 2024a; Yeszhanov et al., 2025), sensor technologies (Pinaeva et al., 2019, 2020; Shakayeva et al., 2023; Zhumanazar et al., 2025), controlled release systems, water-oil separation (Muslimova et al., 2024, 2025; Yeszhanov et al., 2023), and CO_2 capturing and gas separation (Kamakshi et al., 2017; Kumar et al., 2016, 2017; Omertassov et al., 2025; Shakayeva et al., 2025; Usman et al., 2020).

In recent years, various methods have been explored for the deposition of TiO_2 coatings on PET TeMs, aiming to impart photocatalytic, self-cleaning, and antifouling properties while maintaining membrane selectivity and mechanical integrity. Among these methods, reactive magnetron sputtering is the most widely studied and applied technique (Artoshina et al., 2015, 2016; Kravets et al., 2025; Rossouw et al., 2021). It allows the deposition of uniform TiO_2 thin films with good adhesion to polymer substrates, controlled crystallinity, and tunable phase composition (anatase, brookite, amorphous) depending on sputtering parameters such as plasma gas composition, discharge current, substrate temperature, and deposition time.

Planar magnetron sputtering is effective in modifying PET TeMs by forming thin Ti/TiO_2 composite layers, significantly improving membrane hydrophilicity and introducing photocatalytic activity (Rossouw et al., 2021). The use of inverted cylindrical magnetron sputtering further enhances coating uniformity and process stability, which is critical for maintaining the membrane's pore structure (Artoshina et al., 2015). The introduction of metal interlayers (e.g., Ag, Cu) prior to TiO_2 deposition has also been explored to protect the polymer surface from photocatalytic degradation and enhance antibacterial properties (Artoshina et al., 2015, 2016).

At the same time, there are no works related to vacuum-arc ion-plasma deposition of TiO_2 on PET TeMs, although vacuum-arc ion-plasma deposition has emerged as a promising technique due to the high degree of ionization of the vacuum-arc plasma (20–100%), wide working pressure range (10^{-5}–1 Pa), and the flexibility of deposition parameters (discharge current, working gas pressure, substrate bias voltage, etc.), which allow precise control over the structural and physicomechanical properties of the resulting coatings (Kühn-Kauffeldt et al., 2022; Stepanov et al., 2007). In the present study, the vacuum-arc deposition system employed is additionally equipped with a "PINK" gas plasma source combining a heated and hollow cathode, enabling plasma-assisted deposition from a mixed gas-metal plasma.

However, relatively few studies have focused on the formation of thin inorganic films on polymer surfaces deposited by Arc-PVD methods. Other PVD techniques, such as sputtering (including magnetron), electron-beam, or laser-beam evaporation, typically produce atomic vapor fluxes or low-ionization plasma, often resulting in poor adhesion of coatings to polymer substrates. Polymer materials generally exhibit low surface energy and poor adhesion characteristics. To achieve better coating adhesion, surface pre-activation of the polymer is often recommended (Yáñez-Hernández et al., 2025). Nevertheless, achieving uniform, adherent, and mechanically robust TiO_2 coatings on polymer substrates remains a significant challenge.

Arc PVD offers several advantages for depositing dense and adherent TiO_2 coatings at relatively low substrate temperatures, making it suitable for temperature-sensitive polymer membranes. Despite these advantages, limited research has focused on the application of Arc PVD for functionalizing polymer track-etched membranes with TiO_2 coatings. Most existing studies have primarily addressed metallic or ceramic substrates, leaving a knowledge gap regarding the behavior of TiO_2 coatings on TeMs and their impact on membrane performance.

This study addresses this gap by investigating the formation, structure, and functional properties of TiO_2 coatings deposited on polymer track-etched membranes using vacuum-arc ion-plasma spraying. In contrast to conventional magnetron sputtering approaches, this study

explores the use of Arc-PVD for functionalizing polymer membranes and provides a systematic analysis of how deposition parameters influence coating morphology, pore geometry, phase composition, wettability, mechanical properties, and photocatalytic performance. The results provide new insights into the structure–property relationships governing Arc PVD-modified membranes and their potential use in advanced filtration and photocatalytic systems.

2. Methods and Materials

2.1 Materials

Sodium hydroxide, acetic acid, sodium sulfate, and analytical grade hydroquinone were obtained from EKOS (Moscow, Russia). Deionized water (18.2 MΩ·cm) was produced using an Aqvilon D201 purification system (Aqvilon, Moscow, Russia).

2.2 TiO_2 Deposition

Polymer films based on poly(ethylene terephthalate) (PET) with a thickness of 19 μm were irradiated on a heavy-ion accelerator DC-60 using krypton ions with a fluence of 1.0×10^8 ions/cm^2.

Following irradiation, the polymer films were chemically etched in a 2 M NaOH solution at a temperature of 85±0.1 °C, followed by treatment in neutralization solutions (1.0% acetic acid solution) and deionized water.

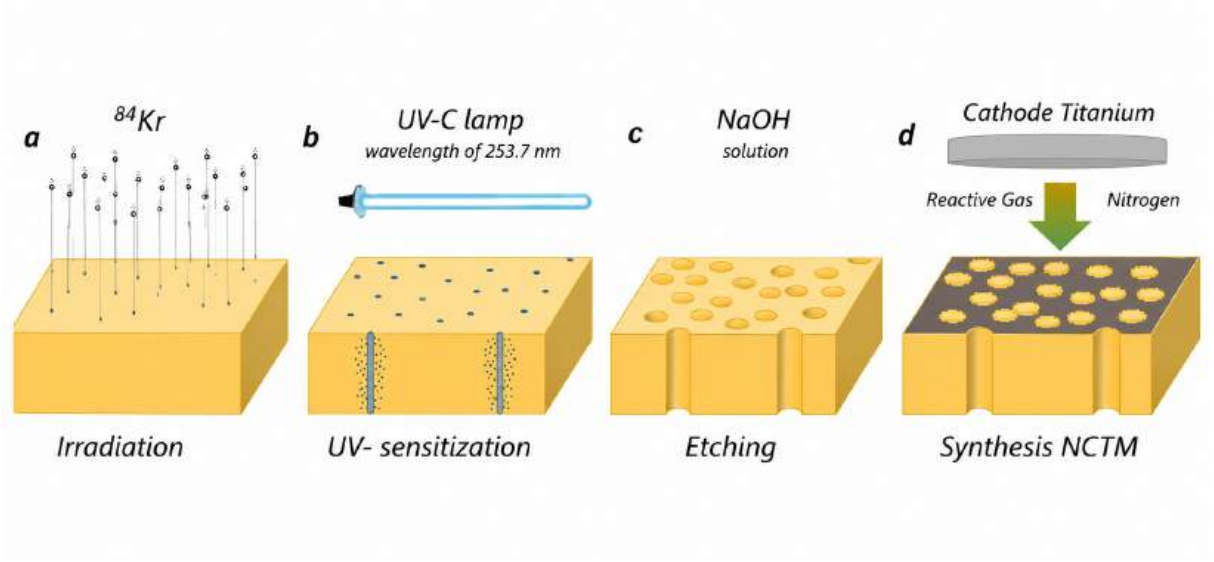

Figure 1 Scheme of the preparation of PET TeMs (irradiation (a), UV-sencibilization (b), Etching (c) and TiO2 deposition (d)

Sample preparation before TiO_2 deposition included cleaning the surface with ethyl alcohol and then rinsing it with deionized water. Then, the membrane was fixed to the surface of a cylindrical fixture equipped with a cooling liquid to prevent polymer membrane overheating using cyanoacrylate glue. To uniformly apply the coating to the membrane, the fixture rotated around its axis at a given speed of $W_0 = 2$ rpm. To apply thin TiO_2 films, a "Bulat" NNV6.6-I1 ion-plasma spraying unit equipped with an evaporator with a magnetic coil and a plasma flow focusing coil was used (Borisov et al., 2007; Khlebnikov et al., 2016). A titanium target (99.77% purity, 80 mm diameter) was used as a cathode. The distance between the substrate and the target was 350 mm. The chamber in which the spraying process took place was evacuated to a pressure of 10^{-5} Pa. The deposition of TiO_2 films took place in an atmosphere of argon and oxygen in a ratio of 2:1 at a pressure of 1 Pa and a negative voltage on the substrate of −80 V during different spraying times: 0.5, 1, 2, 4, and 8 min.

2.3 Sample Characterization

The surface and side chipping studies before and after deposition, as well as the density calculation, were performed in the Marker-12 software using micrographs of the films obtained on a JEOL-7500F scanning electron microscope at a cathode voltage of 2.5 kV, under high vacuum conditions. The size of the nanoparticles forming the coating morphology was determined by measuring the lateral dimensions of the particles using scanning electron microscope software. A sample of 100 nanoparticles was measured for each specimen to assess the particle size distribution. To minimize errors related to inaccuracies in lateral size measurements by scanning electron microscopy (SEM), a sample of at least 70 pores was measured for each specimen. Measurements were taken at five control points across the film width, with an interval of 0.5 mm (three parallel measurements on both the front and reverse sides), and along a film length of at least 1 cm for statistical reliability.

The topographic study of the surfaces of the obtained samples was conducted using an atomic force microscope (AFM) STM SmartSPM, AIST-NT Ltd. Scan mode: AC mode (non-contact mode); scan rate/scan frequency 0.4 Hz, resolution XY 700×700, scan size XY 10×10 μm, Z is automatic; cantilever tip radius is less than 10 nm.

X-ray phase analysis (XRD) was performed on a D8 ADVANCE ECO diffractometer (Bruker, Germany). X-ray diffraction measurements were performed at an accelerating voltage of 20 kV and a beam current of 5 mA in the 2θ range of 20–50°. Under these experimental conditions, the effective penetration depth of X-ray radiation in titanium oxide does not exceed approximately 0.5 μm. The experimental peaks were fitted using an appropriate number of symmetric pseudo-Voigt functions to analyze the diffraction profiles. This approach allowed determination of the full width at half maximum (FWHM), providing insight into the coatings' crystalline quality and structural ordering. The lattice constants were calculated from the most intense reflections of each identified phase using the Nelson–Taylor extrapolation method, and the Scherrer formula was used to estimate the mean crystallite size.

The surface hydrophilicity of the samples was evaluated by measuring the contact angle (θ) using the sessile drop technique. A droplet of the test liquid with a volume of approximately 15 μl was deposited onto the sample surface using a microsyringe. The contact angle was calculated from the geometric parameters of the droplet under the assumption that θ is less than 90° using the following equation:

$$\operatorname{tg}\theta = \frac{2h \cdot r}{r^2 - h^2} \tag{1}$$

where θ is the contact angle, r is the radius of the contact area of the droplet with the surface, and h is the droplet height.

The microhardness of the samples, both before and after coating deposition, was evaluated using a digital LM-700 microhardness tester (Leco Corporation, USA) equipped with a Vickers diamond indenter. The Vickers microhardness (HV) values were obtained under a load of 100 N.

2.4 Photocatalytic Activity of the Samples

The photocatalytic performance of the samples was investigated under ultraviolet light irradiation using a BUV-15 lamp emitting at a wavelength of 253 nm. The photocatalytic activity was assessed by monitoring the oxidation kinetics of a model organic pollutant, p-dihydroxybenzene (hydroquinone, HQ), employed as a probe compound. The working solution for the photo-oxidation experiments was prepared by diluting 1.0 cm^3 of a stock HQ solution (1×10^{-2} M) with 1.5 cm^3 of a 0.5 M sodium sulfate (Na_2SO_4) solution, which served as a supporting electrolyte, followed by the addition of distilled water to a final volume of 25.0 cm^3 in a volumetric flask. The concentration of HQ in the working solution was 4.0×10^{-4} M. The prepared solution was poured into a quartz beaker, where TiO_2-coated polymer PET TeMs with dimensions of 10×10 mm were immersed as photocatalytic substrates and subsequently irradiated with ultraviolet or visible light.

The residual HQ concentration was quantified by voltammetric measurements at specified irradiation time intervals (1–2 h) using a PU-1 polarograph. A cylindrical glassy carbon electrode with an effective surface area of 0.44 cm^2 was employed as the working electrode, while saturated Ag/AgCl electrodes (EVL-1M3 type) were used as both reference and counter electrodes. The potential scan rate was set to 0.030 V s^{-1}. The analytical response corresponded to the oxidation peak of the hydroquinone/quinone redox couple near 0.0 V recorded in differential mode. The photocatalytic experiment was concluded when the HQ concentration either dropped to zero or remained constant despite continuous irradiation.

3. Results and Discussion

3.1 Morphological Study by Scanning Electron Microscopy and Atomic Force Microscopy

SEM image (Figure 2) analysis revealed that a thin monolayer coating of spherical or globular-shaped nanoparticles was formed on the surface of the TeMs at deposition times between 30 and 120 seconds. The openings visible in the SEM images (Figure 2) correspond to the track-etched membrane's through-pore channels. Their presence demonstrates that the Arc-PVD TiO_2 coating conforms to the membrane surface without sealing the pores, thereby preserving permeability and mass transport pathways. Slight narrowing of the pore openings after deposition indicates coating growth along the pore walls rather than pore blockage.

Pore size measurements of both the initial membranes and the coated PET TeMs-TiO_2 showed that the pore diameter remained at 200 nm for deposition times of 30 and 60 seconds, corresponding to the original pore size of the uncoated membranes. However, at 120 seconds, partial pore filling was observed, reducing the diameter to 150 nm. With further increases in deposition time to 240 and 480 seconds, an increasingly non-uniform coating formed on the membrane surface, with significant pore narrowing, and pore diameters decreased to 140 and 90 nm, respectively. This provides the ability to control the pore size during PET TeMs-TiO_2 fabrication. Detailed analysis of the coatings formed at 240 and 480 seconds revealed that the resulting layers were non-uniform and contained cracks and agglomerates.

The results of the particle size and pore analysis are presented in Table 1. According to the presented data, the average nanoparticle size in the coatings obtained at deposition times of 30 and 60 s remained nearly constant at 27±2.5 nm. This behavior can be attributed to rapid nucleation and surface saturation during the early stages of deposition, followed by limited surface diffusion and densification of the coating rather than lateral particle growth. At longer deposition times of 120 and 240 seconds, an increase in particle diameter was observed — 32.5±2.5 nm and 47.5±2.5 nm, respectively. In contrast, when the deposition duration was increased to 480 s, the particle size was reduced. This behavior can be attributed to the emergence of a secondary phase accompanied by modifications in the crystal lattice, as discussed in detail in Section 3.3.

Atomic force microscopy (AFM) in semi-contact mode was employed to evaluate the uniformity and surface development of the coatings (Figure S1), and the measured roughness and waviness parameters are summarized in Table 2. The results demonstrate that increasing coating thickness is accompanied by a systematic increase in both roughness and waviness, reflecting the membrane surface's progressive modification during TiO_2 deposition. This trend indicates a transition from the initial nucleation of nanoparticles to their coalescence and vertical growth, leading to the formation of protruding surface features and increased surface heterogeneity.

The coatings deposited for 4 and 8 min exhibit the largest grain height spread, indicating that prolonged deposition promotes localized crystallization and particle agglomeration within the coating layer. Such behavior is characteristic of ion-plasma deposition processes, where uneven material accumulation is caused by the directional flux of energetic species, shadowing effects near pore edges, and local growth instabilities. As a result, mesoscale surface undulations develop, indicating non-uniform coating thickening and partial densification.

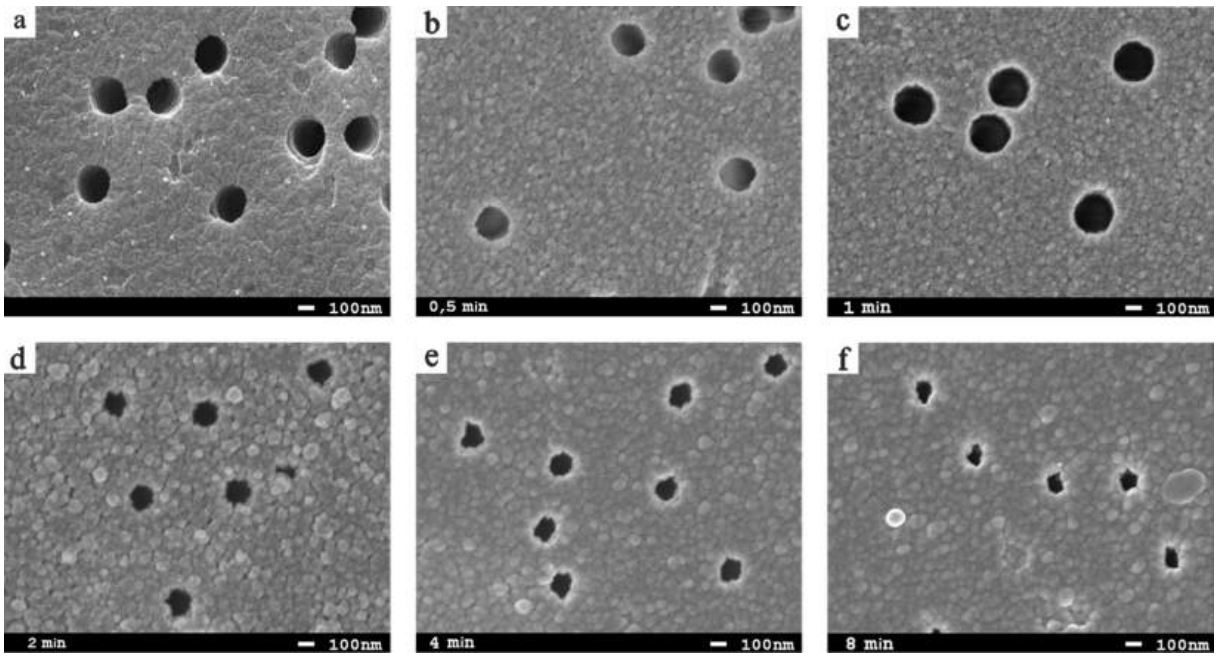

Figure 2 SEM images of the surface of initial PET TeMs (a) and after Arc PVD of TiO_2 during 0.5 min (b), 1 min (c), 2 min (d), 4 min (e), 8 min (f)

The evolution of surface topography has important functional implications. Moderate increases in roughness can enhance the effective surface area and improve light scattering and reactant accessibility, which may benefit photocatalytic reactions. However, excessive agglomeration and waviness can reduce coating uniformity and limit the availability of active surface sites, potentially contributing to reduced photocatalytic efficiency at longer deposition times.

Table 1 Size of TiO_2 nanoparticles, pores of the membranes, Vickers hardness of the coating and contact angle depending on spraying time

Spraying time, min	Nanoparticle diameter, nm	Pore diameter, nm	Vickers hardness of the coating, MPa	CA, °
Initial PET TeMs	–	200	–	68.28±1.11
0.5	27.5 ± 2.5	200	54.2	74.22±1.47
1	27.5 ± 2.5	200	60.8	84.89±1.98
2	32.5 ± 2.5	150	61.6	86.28±1.35
4	47.5 ± 2.5	138	75.2	86.84±1.87
8	40 ± 2.5	93	194.3	88.22±1.21

Table 2 Data from AFM of initial PET TeMs and PET TeMs-TiO_2 obtained at different time

Spraying time, min	Average roughness, nm	Average waviness, nm	Average maximum roughness height, nm
Initial PET TeMs	1.7	4.0	11.6
0.5	2.1	4.7	12.0
1	2.7	7.4	17.4
2	3.0	16.0	27.2
4	3.7	24.1	33.7
8	4.1	25.2	35.1

Surface roughness affects the hydrophilic/hydrophobic properties of membranes (Rezaei et al., 2018). According to theory, as surface roughness increases, so does the contact angle of wetting. The influence of surface modification on wettability and the corresponding changes in the hydrophilic/hydrophobic behavior of the membranes are discussed in detail in Section 3.4.

3.2 Cross-Sectional View of Composite Track-Etched Membranes

Figure S2 shows the lateral fractures of the coated track-etched membranes. The obtained results show that a coating composed of spherical nanoparticles is formed on the surface of the track-etched membranes and within their pores during deposition, with a penetration depth not exceeding 1 μm. Increasing the deposition time results in a thicker nanoparticle layer and a corresponding increase in the average nanoparticle size. This change in size may be attributed to crystallization processes occurring during deposition.

Figure 3 shows the coating thickness as a function of deposition time. We determined the coating thickness by analyzing cross-sectional fractures of the coated TeMs.

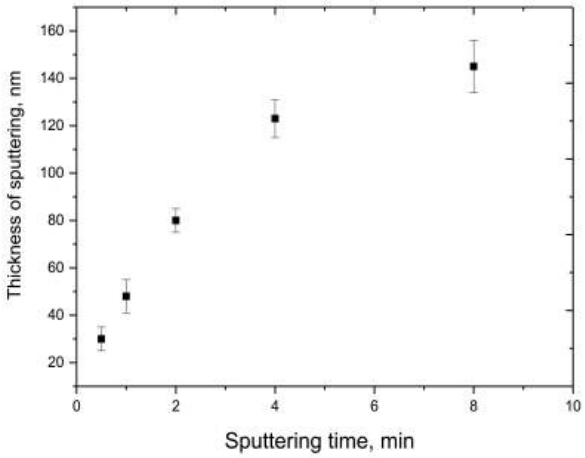

Figure 3 Graph of change in coating thickness with increasing time

The change in coating thickness follows a logarithmic relationship: $y = 44.002\ln(x) + 54.7$. Notably, for deposition times longer than 4 minutes, the increase in coating thickness becomes minimal, which is associated with an increase in coating density. The formation of large droplet-like particles was observed within the coating structure, which may significantly affect the coating morphology and performance characteristics of the PET TeMs-TiO_2.

3.3 Phase Analysis of the Coated Track-Etched Membranes

Figure S3 illustrates the changes in the X-ray diffraction patterns of the samples following coating deposition. The diffraction profiles indicate that the coatings possess a nanoscale polycrystalline structure, which is reflected by the diffraction peaks' low intensity and noticeable broadening. X-ray diffraction (XRD) analysis was employed to identify the phase composition of the coatings and to track the evolution of their crystallographic parameters as a function of deposition time. The results reveal that, for deposition durations ranging from 0.5 to 4 minutes, the deposited layer consists predominantly of polycrystalline anatase TiO_2 with a tetragonal crystal structure (space group $I4_1/amd$ (141)).

The relatively low crystallinity of the TiO_2 coatings can be attributed to the low substrate temperature required to prevent thermal damage to the polymer membrane, which limits crystal growth. In addition, the short deposition time and small coating thickness result in the formation of nanocrystalline domains with broadened diffraction peaks. The amorphous nature of the PET substrate further restricts crystalline growth due to the absence of epitaxial ordering.

Table 3 Calculated crystallographic characteristics

Spraying time, min	Phase	Crystal lattice parameters, Å	Average crystallite size, nm	Degree of crystallinity, %
0.5	TiO_2 - anatase	$a = 3.82865$, $c = 9.13812$	5.3 ± 0.3	13
1	TiO_2 - anatase	$a = 3.81739$, $c = 9.12199$	5.8 ± 0.3	21
2	TiO_2 - anatase	$a = 3.82712$, $c = 9.13451$	6.5 ± 0.4	25
4	TiO_2 - anatase	$a = 3.82487$, $c = 9.12914$	7.1 ± 0.5	31
8	TiO_2 - anatase	$a = 3.82712$, $c = 9.10229$	7.2 ± 0.3	44
	TiO_2 - brookite	$a = 9.16860$, $b = 5.45862$, $c = 5.14707$	5.5 ± 0.1	–

Prolongation of the deposition process results in the emergence of an additional preferred orientation corresponding to the (211) crystallographic plane, reflecting an increase in the thickness of the deposited coating. When the deposition time is further extended to 8 minutes, a secondary brookite TiO_2 phase with an orthorhombic crystal structure (space group Pbca (161)) is detected. This additional phase formation can be attributed to the increased coating thickness and phase transformations occurring during film growth. Table 3 shows a summary of the extracted crystallographic parameters.

It should be emphasized that longer deposition times, and thus greater coating thicknesses, promote an increase in both the surface layer's average crystallite size and overall crystallinity. This improvement in crystallinity is associated with the formation of a more ordered crystal lattice, a decrease in the number of structurally disordered regions, and densification of the coating.

Variations in the calculated lattice parameters indicate lattice contraction accompanied by material density changes. The density of the deposited layer was determined using Equation 2:

$$p = \frac{1.6602 \sum AZ}{V_o}, \tag{2}$$

where $V_0 = \frac{\sqrt{3}}{2} a^2 c$ is the unit cell volume, Z is the number of atoms per unit cell, A is the atomic weight of the atoms, and N_A is Avogadro's number. Figure 4a shows the evolution of the density of the deposited layer as a function of deposition time.

The observed crystal lattice contraction is accompanied by a decrease in the unit cell volume and a corresponding densification of the deposited layer. The increase in density reduces disordered regions within the structure, confirming the enhanced degree of crystallinity. Figure 4b shows the dislocation density evolution as a function of deposition time. Dislocation densities of the order of $\sim 10^{15}$ m^{-2} are characteristic of highly deformed crystal lattices. A decrease in the dislocation density within the crystalline lattice improves the mechanical strength. The increase in the average crystallite size and the reduction of disordered regions contribute to a decrease in the dislocation density, which subsequently reduces the lattice strain and macrostress. Macrostress was evaluated based on the analysis of diffraction peak shifts, and the results are presented in Table S1.

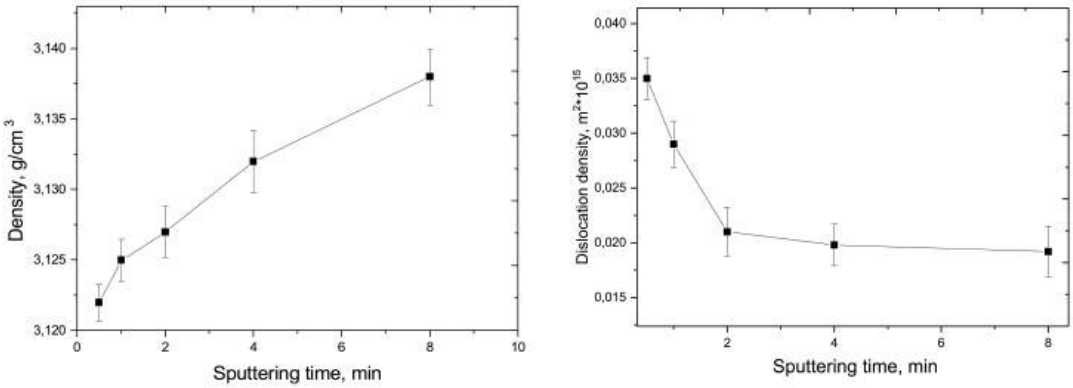

Figure 4 (a) Evolution of the deposited layer density as a function of deposition time and (b) dislocation density as a function of deposition time

An increase in the spraying duration results in higher crystallinity and density of the deposited layer, which in turn reduces macrostresses within the crystal lattice. The key mechanical properties of the coatings are their hardness and mechanical strength. The Vickers hardness of the deposited layers was calculated using Equation 3:

$$HV = 0.0018544 \cdot \frac{P}{d^2} \tag{3}$$

where P is the applied load (N), and d is the length of the indentation's long diagonal left by the indenter (mm). The results are presented in Table 2. An increase in the crystallinity degree and coating thickness leads to an increase in coating hardness and, consequently, to improved mechanical strength.

The results demonstrate that higher crystallinity and greater coating thickness are associated with the enhanced mechanical strength of the deposited layer. These observations agree well with the trends and analyses discussed in the preceding sections.

3.4 Water Contact Angle Study

To evaluate the effect of coating on the hydrophilic properties of track-etched membranes, the contact angle and surface roughness were measured, and the mechanical properties were determined. Table 2 summarizes the calculated contact angle values. The data indicate that an increase in coating thickness is accompanied by an increase in the contact angle, which corresponds to the enhanced hydrophobic behavior of the membrane surface.

At the same time, increasing the deposition time from 4 to 8 minutes results in only a slight change in the contact angle. The change in the contact angle may be attributed to alterations in the surface morphology and roughness of the track-etched membranes with and without coating.

3.5 Study of the Photocatalytic Properties of PET TeMs-TiO_2

It is well known that titanium oxide phases exhibit photocatalytic activity under UV irradiation (Leong et al., 2014). To investigate the influence of coating thickness on the functional properties of the obtained samples, we studied the photocatalytic activity of flat TiO_2-coated MTEM (anatase–brookite) samples toward an aqueous solution of HQ (hydroquinone) at pH 6.8 and 22°C. The experimental results are presented in Figure 5. The kinetic curves show that the change in the substrate concentration in the solution follows first-order irreversible reaction kinetics over the entire concentration range. Figure 5b presents the empirical dependence of the substrate decomposition rate constant on the TiO_2 coating deposition time. As the number of irradiation cycles increases, the reaction rate decreases. By comparing the relationship between TiO_2 coating thickness and the photocatalytic oxidation rate of HQ as a function of deposition time, the most effective concentration of the TiO_2 photocatalyst corresponds to the coating

thicknesses obtained at deposition times of 30–120 s. Under UV irradiation, the TiO_2 coatings exhibited weak photocatalytic activity, which was only slightly dependent on the film thickness.

The photocatalytic oxidation data show that the maximum HQ oxidation rate is achieved with the TiO_2 film deposited for 120 seconds. Under these conditions, the HQ oxidation rate is comparable to that obtained using the reference TiO_2 material (Degussa). As the TiO_2 deposition time (and hence the film thickness) increases, the photocatalytic oxidation rate decreases. To evaluate the stability of the samples as photocatalysts, two oxidation cycles were conducted on the same TiO_2 film surface. During the second cycle, the HQ oxidation rate decreased to a level comparable to that of HQ oxidation without a catalyst. Overall, the photocatalytic oxidation rate slightly decreases with increasing coating thickness (see Figure 5d).

The observed decrease in photocatalytic activity with increasing TiO_2 deposition time (and corresponding film thickness) can be explained by several interrelated factors. First, thicker TiO_2 layers limit UV light penetration, reducing the effective photoactive volume and photon utilization efficiency (Leong et al., 2014). Second, increasing film thickness promotes the recombination of photogenerated electron–hole pairs due to longer charge transport pathways, which decreases the formation of reactive oxygen species responsible for pollutant degradation (Fujishima et al., 2008). In addition, SEM and AFM analyses indicate particle growth, agglomeration, and coating densification at longer deposition times, reducing the accessible surface area and number of active catalytic sites. Partial pore narrowing and filling further hinder the mass transport of reactants toward the catalytic surface.

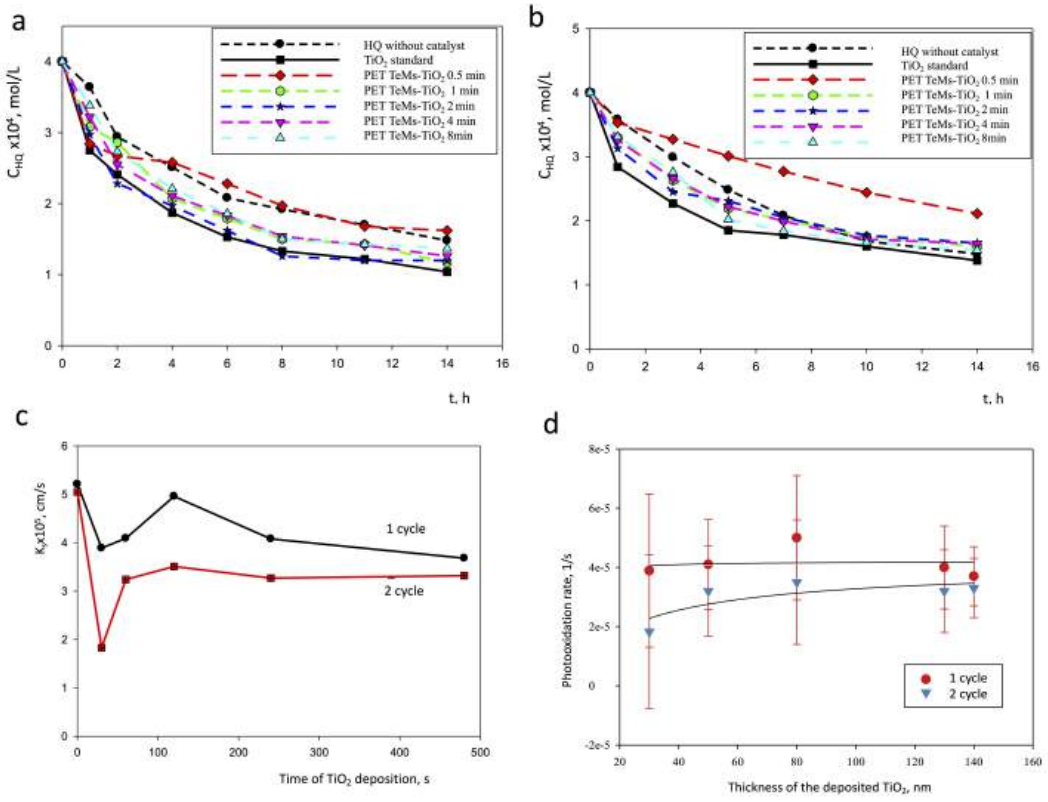

Figure 5 Change in hydroquinone concentration under UV irradiation on PET TeMs-TiO_2 (synthesis 2), first cycle (a), change in hydroquinone concentration under UV irradiation on TiO_2 films (synthesis 2), second cycle (b), dependence of the HQ oxidation rate constant under UV irradiation on TiO_2 film thickness over two oxidation cycles (c) and effect of TiO_2 coating thickness on the photocatalytic oxidation rate of HQ (d)

In addition to the observed improvements in surface properties and photocatalytic performance, the combination of controlled pore geometry and photocatalytic TiO_2 coatings makes the developed membranes promising for photocatalytic water purification and antifouling filtration

systems. The ability to degrade organic contaminants under UV irradiation may also enable self-cleaning functionality and extended membrane lifetime, thereby improving operational stability and reducing maintenance requirements.

4. Conclusions

Thin TiO_2 coatings were successfully deposited on PET track-etched membranes using Arc-PVD at deposition times ranging from 0.5 to 8 min. SEM and AFM analyses showed progressive pore constriction from 200 to 93 nm with increasing deposition time, accompanied by particle growth and changes in surface topography, reflected in increased roughness (1.7–4.1 nm) and waviness (4–25.2 nm). The cross-sectional observations revealed a logarithmic growth behavior of the coating thickness, indicating gradual densification of the layer during deposition. XRD analysis confirmed the formation of polycrystalline anatase TiO_2 at shorter deposition times, while a secondary brookite phase appeared at prolonged deposition (8 min). Increasing the deposition time reduced the lattice strain and dislocation density, contributing to improved mechanical properties and increased coating hardness. The contact angle increased from 68° to 88°, indicating decreased surface wettability. Under UV irradiation, the TiO_2 coatings exhibited nonlinearly dependent photocatalytic activity on film thickness, with the highest hydroquinone oxidation rate observed at a deposition time of 120 s, comparable to the benchmark Degussa TiO_2. Overall, Arc-PVD modification enables controlled tuning of pore geometry, surface properties, and photocatalytic performance, demonstrating its feasibility for functionalizing polymer track-etched membranes.

Acknowledgements

This research was funded by the Ministry of Science and Higher Education of the Republic of Kazakhstan (BR28713053).

Author Contributions

Conceptualization, I.E.K., N.A.K. and N.R.B.; methodology, N.A.K., A.B.Y. and E.V.P.; validation, N.Z., A.B.Y. and A.K.S.; investigation, I.V.K., I.E.K., N.Z. and A.K.S.; resources, I.E.K., N.Z. and A.B.Y.; data curation, N.R.B. and A.K.S.; writing—original draft preparation, I.V.K., I.E.K. and N.Z.; writing—review and editing, E.V.P., N.A.K. and N.R.B.; visualization, N.A.K.; supervision, N.A.K. and E.V.P.; project administration, I.V.K. and N.A.K.; funding acquisition, I.V.K. All authors have read and agreed to the published version of the manuscript.

Conflict of Interest

The authors declare no conflicts of interest.

Supplementary Materials

Figure S1 — AFM images of the surface of initial PET TeMs and after TiO_2 deposition at different times; Figure S2 — SEM images of cross-sectional views; Figure S3 — X-ray diffraction patterns of the investigated samples PET TeMs-TiO_2 obtained at different deposition time; Table S1 — Data on macrostresses in the crystal lattice of the samples.

Declaration of AI

In preparing this manuscript, the authors utilized Grammarly and ChatGPT-4o to enhance the English grammar and style for improved clarity and readability. The original draft and subsequent revisions were written by the authors themselves. Following the use of these tools, the authors thoroughly reviewed and edited the output and assume full responsibility for the final content of this publication.

References

Apel, P. Y. (2019). Fabrication of functional micro- and nanoporous materials from polymers modified by swift heavy ions. *Radiation Physics and Chemistry*, *159*, 25–34. https://doi.org/10.1016/j.radphyschem.2019.01.009

Apel, P. Y., Blonskaya, I. V., Lizunov, N. E., Olejniczak, K., Orelovitch, O. L., Toimil-Molares, M. E., & Trautmann, C. (2018). Osmotic effects in track-etched nanopores. *Small*, *14*(18), 1703327. https://doi.org/10.1002/smll.201703327

Artoshina, O. V., Milovich, F. O., Rossouw, A., Gorberg, B. L., Iskhakova, L. D., Ermakov, R. P., Semina, V. K., Kochnev, Y. K., et al. (2016). Structure and phase composition of thin TiO2 films grown on the surface of metallized track-etched polyethylene terephthalate membranes by reactive magnetron sputtering. *Inorganic Materials*, *52*(9), 945–954. https://doi.org/10.1134/S0020168516080021

Artoshina, O. V., Rossouw, A., Semina, V. K., Nechaev, A. N., & Apel, P. Y. (2015). Structural and physicochemical properties of titanium dioxide thin films obtained by reactive magnetron sputtering, on the surface of track-etched membranes. *Petroleum Chemistry*, *55*(10), 759–768. https://doi.org/10.1134/S0965544115100011

Benmalek, M., & Dunlop, H. M. (1995). Inorganic coatings on polymers. *Surface and Coatings Technology*, *76–77*, 821–826. https://doi.org/10.1016/0257-8972(95)02601-0

Borisov, S. V., Polyakov, E. V., & Khlebnikov, N. A. (2007). Patent RU2007139120A [Available from: https://patents.google.com/patent/RU2007139120A/en [Accessed 23 February 2026]].

Fujishima, A., Zhang, X., & Tryk, D. A. (2008). TiO2 photocatalysis and related surface phenomena. *Surface Science Reports*, *63*(12), 515–582. https://doi.org/10.1016/j.surfrep.2008.10.001

Kamakshi, Kumar, R., Saraswat, V. K., Kumar, M., & Awasthi, K. (2017). Palladium nanoparticle binding in functionalized track etched PET membrane for hydrogen gas separation. *International Journal of Hydrogen Energy*, *42*(25), 16186–16194. https://doi.org/10.1016/j.ijhydene.2017.05.040

Khlebnikov, N., Polyakov, E., Borisov, S., Barashev, N., Biramov, E., Maltceva, A., Vereshchagin, A., Khartov, S., et al. (2016). Composite materials obtained by the ion–plasma sputtering of metal compound coatings on polymer films. *Japanese Journal of Applied Physics*, *55*(1S), 01AG02. https://doi.org/10.7567/JJAP.55.01AG02

Kravets, L., Vinogradov, I., Rossouw, A., Gorberg, B., Nechaev, A., & Apel, P. (2025). Functionalization of PET track-etched membranes with electrospun PVDF nanofibers for hybrid membranes fabrication in water desalination. *Separation and Purification Technology*, *371*, 133395. https://doi.org/10.1016/J.SEPPUR.2025.133395

Kühn-Kauffeldt, M., Kühn, M., Mallon, M., Saur, W., & Fuchs, F. (2022). Vacuum arc plasma coating for polymer surface protection — a plasma enhanced in-orbit additive manufacturing concept. *Plasma*, *5*(4), 470–481. https://doi.org/10.3390/plasma5040035

Kumar, R., Kamakshi, Kumar, M., & Awasthi, K. (2016). Functionalized pd-decorated and aligned MWCNTs in polycarbonate as a selective membrane for hydrogen separation. *International Journal of Hydrogen Energy*, *41*(48), 23057–23066. https://doi.org/10.1016/j.ijhydene.2016.09.008

Kumar, R., Kamakshi, Kumar, M., & Awasthi, K. (2017). Selective deposition of pd nanoparticles in porous PET membrane for hydrogen separation. *International Journal of Hydrogen Energy*, *42*(22), 15203–15210. https://doi.org/10.1016/j.ijhydene.2017.03.202

Le, T. M. H., Chuchak, R., & Sairiam, S. (2024). Empowering TiO2–coated PVDF membranes stability with polyaniline and polydopamine for synergistic separation and photocatalytic enhancement in dye wastewater purification. *Scientific Reports*, *14*(1), 15969. https://doi.org/10.1038/s41598-024-66996-w

Leong, S., Razmjou, A., Wang, K., Hapgood, K., Zhang, X., & Wang, H. (2014). TiO2 based photocatalytic membranes: A review. *Journal of Membrane Science*, *472*, 167–184. https://doi.org/10.1016/J.MEMSCI.2014.08.016

Li, C., Yu, H., Huang, B., Liu, G., Guo, Y., Zhu, H., & Yu, B. (2023). Fabrication of anatase TiO2/PVDF composite membrane for oil-in-water emulsion separation and dye photocatalytic degradation. *Membranes*, *13*(3), 364. https://doi.org/10.3390/membranes13030364

Matsudo, A., Oliveira, L. V. F., Martins, T. S., & Camilo, F. F. (2024). Eco-friendly photocatalytic solutions: Synthesized TiO2 nanoparticles in cellulose membranes for enhanced degradation of indigo carmine dye. *ACS Omega*, *9*(43), 43395–43405. https://doi.org/10.1021/acsomega.4c04017

Muslimova, I. B., Omertassov, D. D., Zhumanazar, N., Assan, N., Zhatkanbayeva, Z. K., & Korolkov, I. V. (2025). Preparation of ph-responsive PET TeMs by controlled graft block copolymerisation of styrene and methacrylic acid for the separation of water–oil emulsions. *Polymers*, *17*(16), 1–20. https://doi.org/10.3390/polym17162221

Muslimova, I. B., Zhumanazar, N., Melnikova, G. B., Yeszhanov, A. B., Zhatkanbayeva, Z. K., Chizhik, S. A., Zdorovets, M. V., Güven, O., et al. (2024). Preparation and application of stimuli-responsive PET TeMs: RAFT graft block copolymerisation of styrene and acrylic acid for the separation of water–oil emulsions. *RSC Advances*, *14*(20), 14425–14437. https://doi.org/10.1039/D4RA02117G

Omertassov, D. D., Shakayeva, A. K., Zhatkanbayeva, Z. K., Shakirzyanov, R. I., Zdorovets, M. V., Güven, O., & Korolkov, I. V. (2025). HKUST-1 synthesis in PET track-etched membranes via conversion of deposited Cu for carbon dioxide capture. *ACS Omega*, *10*, 30259–30271. https://doi.org/10.1021/acsomega.5c01493

Pinaeva, U., Dietz, T. C., Al Sheikhly, M., Balanzat, E., Castellino, M., Wade, T. L., & Clochard, M. C. (2019). Bis[2-(methacryloyloxy)ethyl] phosphate radiografted into track-etched PVDF for uranium (vi) determination by means of cathodic stripping voltammetry. *Reactive and Functional Polymers*, *142*, 77–86. https://doi.org/10.1016/j.reactfunctpolym.2019.06.006

Pinaeva, U., Ollier, N., Cavani, O., Balanzat, E., Al-Sheikhly, M., Wade, T. L., & Clochard, M. C. (2020). An uranyl sorption study inside functionalised nanopores. *Scientific Reports*, *10*(1), 1–10. https://doi.org/10.1038/s41598-020-62792-4

Rezaei, M., Warsinger, D. M., Lienhard V, J. H., Duke, M. C., Matsuura, T., & Samhaber, W. M. (2018). Wetting phenomena in membrane distillation: Mechanisms, reversal, and prevention. *Water Research*, *139*, 329–352. https://doi.org/10.1016/J.WATRES.2018.03.058

Rossouw, A., Kristavchuk, O., Olejniczak, A., Bode-Aluko, C., Gorberg, B., Nechaev, A., Petrik, L., Perold, W., et al. (2021). Modification of polyethylene terephthalate track etched membranes by planar magnetron sputtered Ti/TiO2 thin films. *Thin Solid Films*, *725*, 138641. https://doi.org/10.1016/J.TSF.2021.138641

Shakayeva, A. K., Munasbaeva, K. K., Zhumazhanova, A. T., Zdorovets, M. V., & Korolkov, I. V. (2023). Electrochemical sensors based on modified track–etched membrane for non-enzymatic glucose determination. *Microchemical Journal*, *193*, 109003. https://doi.org/10.1016/j.microc.2023.109003

Shakayeva, A. K., Omertassov, D. D., Zhatkanbayeva, Z. K., Shakirzyanov, R. I., Zhumazhanova, A. T., & Korolkov, I. V. (2025). Metal–organic framework-immobilized track-etched membrane with PVC nanofiber mats for carbon dioxide capture. *RSC Advances*, *15*, 37348–37360. https://doi.org/10.1039/D5RA04733A

Shakayeva, A. K., Yeszhanov, A. B., Borissenko, A. N., & Kassymzhanov, M. T. (2024a). Surface modification of polyethylene terephthalate track-etched membranes for application in water desalination by direct contact membrane distillation. *Membranes*, *14*, 145. https://doi.org/10.3390/membranes14070145

Shakayeva, A. K., Yeszhanov, A. B., Zhumazhanova, A. T., Korolkov, I. V., & Zdorovets, M. V. (2024b). Fabrication of hydrophobic PET track-etched membranes using 2,2,3,3,4,4,4-heptafluorobutyl methacrylate for water desalination by membrane distillation. *Eurasian Journal of Chemistry*, *29*, 81–88. https://doi.org/10.31489/2959-0663/2-24-5

Stepanov, I. B., Ryabchikov, A. I., Nochovnaya, N. A., Sharkeev, Y. P., Shulepov, I. A., Ryabchikov, I. A., Sivin, D. O., & Fortuna, S. V. (2007). Vacuum arc filtered metal plasma application in hybrid technologies of ion-beam and plasma material processing. *Surface and Coatings Technology*, *201*(19–20), 8596–8600. https://doi.org/10.1016/J.SURFCOAT.2006.09.320

Usman, M., Ali, M., Al-Maythalony, B. A., Ghanem, A. S., Saadi, O. W., Ali, M., Jafar Mazumder, M. A., Abdel-Azeim, S., et al. (2020). Highly efficient permeation and separation of gases with metal-organic frameworks confined in polymeric nanochannels. *ACS Applied Materials & Interfaces*, *12*(44), 49992–50001. https://doi.org/10.1021/acsami.0c13715

Vilenskii, A. I., Sabbatovskii, K. G., Sobolev, V. D., & Mchedlishvili, B. V. (2013). Electrophysical properties of latent tracks of heavy ions in polymers. *Colloid Journal*, *75*(6), 628–633. https://doi.org/10.1134/S1061933X13060185

Wen, Q., Yan, D., Liu, F., Wang, M., Ling, Y., Wang, P., Kluth, P., Schauries, D., et al. (2016). Highly selective ionic transport through subnanometer pores in polymer films. *Advanced Functional Materials*, *26*(32), 5796–5803. https://doi.org/10.1002/adfm.201601689

Werber, J. R., Osuji, C. O., & Elimelech, M. (2016). Materials for next-generation desalination and water purification membranes. *Nature Reviews Materials*, *1*(5), 16018. https://doi.org/10.1038/natrevmats.2016.18

Yáñez-Hernández, L. A., Bonilla-Gameros, L., Chevallier, P., Sarkissian, A., & Mantovani, D. (2025). Plasma-Based amorphous carbon coatings on polymeric substrates for biomedical applications: A critical review focused on adhesion. *Applied Sciences*, *15*(18), 9968. https://doi.org/10.3390/app15189968

Yeszhanov, A. B., Korolkov, I. V., Shakayeva, A. K., Lissovskaya, L. I., & Zdorovets, M. V. (2023). Preparation of poly(ethylene terephthalate) track-etched membranes for the separation of water-oil emulsions. *Eurasian Journal of Chemistry*, *110*(2), 131–138. https://doi.org/10.31489/2959-0663/2-23-5

Yeszhanov, A. B., Shakayeva, A. K., Zdorovets, M. V., Borgekov, D. B., Kozlovskiy, A. L., Kharkin, P. V., Zheltov, D. A., Krasnopyorova, M. V., et al. (2025). Hybrid membranes based on track-etched membranes and nanofiber layer for water–oil separation and membrane distillation of low-level liquid radioactive wastes and salt solutions. *Membranes*, *15*(7), 1–16. https://doi.org/10.3390/membranes15070202

Zhumanazar, N., Yeszhanov, A. B., Melnikova, G. B., Zhumazhanova, A. T., Chizhik, S. A., & Korolkov, I. V. (2025). Electrochemical sensors based on track-etched membranes for rare earth metal ion detection. *ChemEngineering*, *9*(4), 1–15. https://doi.org/10.3390/chemengineering9040088